
A simple probabilistic deep generative model for learning generalizable disentangled representations from grouped data

Haruo Hosoya

ATR International, Kyoto, Japan

hosoya@atr.jp

Abstract

The disentangling problem is to discover multiple complex factors of variations hidden in data. One recent approach is to take a dataset with grouping structure and separately estimate a factor common within a group (content) and a factor specific to each group member (transformation). Notably, this approach can learn to represent a continuous space of contents, which allows for generalization to data with unseen contents. In this study, we aim at cultivating this approach within probabilistic deep generative models. Motivated by technical complication in existing group-based methods, we propose a simpler probabilistic method, called group-contrastive variational autoencoders. Despite its simplicity, our approach achieves reasonable disentanglement with generalizability for three grouped datasets of 3D object images. In comparison with a previous model, although conventional qualitative evaluation shows little difference, our qualitative evaluation using few-shot classification exhibits superior performances for some datasets. We analyze the content representations from different methods and discuss their transformation-dependency and potential performance impacts.

1 Introduction

Human can effortlessly disentangle complex factors of variations in sensory inputs. For example, when seeing a set of face images like in Figure 1A, we can easily recognize that the explaining factors are the content—

what the face is shaped like—and the transformation—how the face is posed or expressing. Furthermore, once we discover the factors, we can generalize this knowledge for faces of unseen identities. How can such ability be achieved computationally?

The disentanglement problem has recently been attracting much attention in the context of deep generative models (Kingma and Welling (2014); Goodfellow et al. (2014)). Among others, one promising approach is to use a dataset that comes with grouping structure (Mathieu et al. (2016); Bouchacourt et al. (2018); Chen et al. (2018)). That is, when data items (like images) containing the same content but transformed differently are grouped together, effective disentanglement can be achieved by extracting the content as the factor common within a group and the transformation as the factor differentiating the group members.¹ Notably, this approach allows for generalization over novel contents: the learned representation forms a general continuous “space” of contents (e.g., a space of facial shapes), which can accommodate unseen contents. Such generalizability is not commonly attainable, in particular, in approaches that only separate classes from transformations (Kingma et al. (2014); Cheung et al. (2014); Siddharth et al. (2017); Chen et al. (2016)).

The purpose of this study is to further pursue the group-based approach within a probabilistic generative model. We here develop a new method called group-contrastive variational autoencoders (GVAE), extending variational autoencoders (VAE; Kingma and Welling (2014)). The main motivation is that previous methods of the same goal (Mathieu et al. (2016); Bouchacourt et al. (2018)) have used rather complicated techniques for exploiting the grouping structure but necessity of such complexity has been unclear. For example, Mathieu et al. (2016) used adversarial learn-

¹Such assumption is not abnormal since a grouped dataset would easily be derived from class-labeled data (by grouping images of the same class) or from video data (by grouping frames in the same or nearby sequence); e.g., Figure 1A.

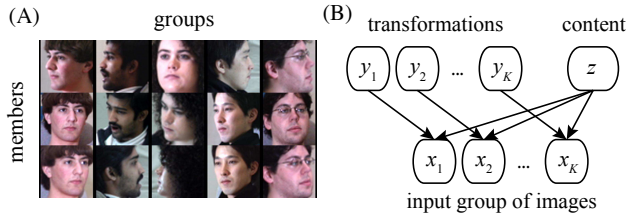


Figure 1: (A) Example of grouped data. Each column groups face images of the same person with different views. (B) The graphical model. Each group member x_k is generated from the member-specific transformation variable y_k and the member-general content variable z .

ing in combination with VAE, requiring optimization of multiple objectives; Bouchacourt et al. (2018) used “evidence accumulation” technique for encoding contents in a VAE-based model, involving complex multiplication of deep net outputs in the objective. In contrast, we use only a simple “averaging” of individual content representations to obtain the common content, which is technically not much more than the basic VAE, yet achieve reasonable disentanglement and generalizability over novel contents.

To evaluate our approach, we concentrate here on comparison with Multi-Level VAE (MLVAE; Bouchacourt et al. (2018)), which is the closest method to ours. We introduce a quantitative evaluation method using few-shot classification. The rationale is: since a successful representation would cleanly separate content from transformation, it would achieve high performance in classifying test data of novel classes using a small number of examples. While conventional qualitative evaluation indicates little discernible difference between GVAE and MLVAE, our quantitative evaluation shows significant superiority of GVAE for some datasets. For further understanding, we analyze the latent representations and expose the way of coding uncertainty in MLVAE that leads to transformation-dependent representations, potentially conflicting with the goal of disentanglement.

2 Related work

As already mentioned, several studies have investigated disentanglement using grouped data. Mathieu et al. (2016) have proposed a combination of VAE and generative adversarial networks (GAN; Goodfellow et al. (2014)). They used adversarial learning as a regularization to encourage generated images to be classified as the same when changing the transformation factor. They verbally reported that omitting adversarial learning abol-

ished disentanglement, although we show here that it can be achieved without such technique; we believe that this is because we chose a very low dimension for the transformation variable (Section 5.1). In addition, although they pointed out the potential of this approach for generalization over new contents, they demonstrated it only for one dataset with a rather unclear result possibly due to the small data size. The more recent study by Bouchacourt et al. (2018), developed concurrently with ours, proposed MLVAE, which estimates the common content using evidence accumulation; we provide detailed comparison in Section 5. Chen et al. (2018) have extended GAN for disentanglement from grouped data. Although their method is simple yet powerful enough to learn content-transformation separation and generate clean and sharp images. However, we should stress that GAN-based approaches usually do not offer a probabilistic generative model (in the form of a joint distribution of input and latent variables) and therefore cannot enjoy the flexibility and extensibility that otherwise come for free (semi-supervised learning, partial observation, etc.).

Grouped data are related to sequential data like video. Yang et al. (2015) and Denton and Birodkar (2017) have investigated disentanglement for video data. They crucially assumed that the content variable remains similar in consecutive frames, as inspired by the temporal coherence principle (Földiák (1991)). Although this idea itself is somewhat similar to the group-based approach, the sequence-based methods have used additional mechanisms to exploit ordering among data items, e.g., a recurrent neural network to predict future states from past states (Yang et al. (2015)) or adversarial training to take temporal structure into account (Denton and Birodkar (2017)).

Supervised or semi-supervised approaches can also achieve effective disentanglement by explicitly supplying the content information and inferring the transformation variable as the remaining factor (Kingma et al. (2014); Cheung et al. (2014); Siddharth et al. (2017)). However, the prior studies in this approach have typically supplied class labels for supervision (since these are the only labels available in most datasets), represented them in categorical variables, and estimated a generative model conditioned on the class. Since such estimated model would have little useful information for unseen classes, generalization for new contents seems difficult.

Some unsupervised approaches require no label or grouping in data, but optimize the efficiency of the latent representation, either by maximizing mutual information between hidden variables in a GAN-based model (Chen et al. (2016)) or by adjusting a so-called β -term in a variational lower bound (Higgins et al.

(2016)). Either study focused on disentangling capability, but not generalizability over novel contents.

3 Method

3.1 Model

We assume a dataset \mathcal{D} consisting of N groups, in which each group has K data members, $(x_1^{(n)}, \dots, x_K^{(n)})$, where $x_k^{(n)} \in \mathcal{R}^D$ is a data member indexed by the group number n and the member number k . For example, Figure 1A shows a set of 5 groups of 3 data members, where each member is an image. (For brevity, we sometimes elide the superscript (n) below.) We assume independence between groups but not members within a group. We intend that each group in the dataset contains different transformations of the same content. (We do not require alignment in transformation at each group member number.) In other words, the factor common among the group members correspond to the content, while the factor differentiating them correspond to the transformation.

To extract such common and differentiating factors from the grouped data, we consider the following probabilistic generative model with two types of hidden variables: the (member-specific) transformation variables $y_1, \dots, y_K \in \mathcal{R}^L$ and the (member-common) content variable $z \in \mathcal{R}^M$ (Figure 1B):

$$p(z) = \mathcal{N}(0, I) \quad (1)$$

$$p(y_k) = \mathcal{N}(0, I) \quad (2)$$

$$p_\theta(x_k|y_k, z) = \mathcal{N}(f_\theta(y_k, z), I) \quad (3)$$

for $k = 1, \dots, K$. That is, each hidden variable, z or y_k , is generated from the standard Gaussian prior. Then, each observed variable x_k is generated from the decoder f_θ applied to the corresponding individual transformation y_k and the common content z , added with Gaussian noise of unit variance, where the decoder f_θ is a deep net with weight parameters θ .

3.2 GVAE

For learning, we extend the VAE approach introduced by Kingma and Welling (2014), which uses encoder models based on deep nets to approximate posterior distributions for hidden variables. First, we estimate each transformation y_k from the corresponding input image x_k as follows:

$$q_{\phi, \xi}(y_k|x_k) = \mathcal{N}(g_\phi(x_k), r_\xi(x_k)) \quad (4)$$

where we use an encoder deep net g_ϕ with weight parameters ϕ for estimating the mean and another deep net r_ξ (positively valued) with weight parameters ξ for

estimating the variance. For inference of content, we could likewise assume a pair of deep nets to estimate the content z from all images x_1, \dots, x_K , but it cannot exploit symmetry in the members of the same group. Instead, our approach estimates the individual content for each image x_k by a pair of deep nets and thereafter averages all the individual contents to obtain the common content z :

$$q_{\psi, \pi}(z|x_1, \dots, x_K) = \mathcal{N}\left(\frac{1}{K} \sum_{k=1}^K h_\psi(x_k), \frac{1}{K} \sum_{k=1}^K s_\pi(x_k)\right) \quad (5)$$

The encoder deep nets h_ψ and s_π each estimate the mean and variance of the posterior distribution of an individual content. The common content z for all group members is inferred as the average of the individual contents. Note that, therefore, the variance of z becomes the average of the individual variances. The intention here is that, as we attempt to reconstruct each image x_k by the common content z with the individual transformation y_k , all the individual contents $h_\psi(x_1), \dots, h_\psi(x_K)$ are encouraged to converge to an equal value in the course of learning. Thus, z will eventually become a common factor of all x_k , while each y_k will become a differentiating factor.

To train the model, we consider the following variational lower bound of the log likelihood:

$$\begin{aligned} \log p_\theta(\mathbf{x}) &\geq \mathcal{E}_{q_{\theta, \phi, \xi, \psi, \pi}(\mathbf{y}, z|\mathbf{x})} \left[\sum_{k=1}^K \log p_\theta(x_k|y_k, z) \right] \\ &\quad - \sum_{k=1}^K \text{KL}(q_{\phi, \xi}(y_k|x_k) \| p(y_k)) \\ &\quad - \text{KL}(q_{\psi, \pi}(z|\mathbf{x}) \| p(z)) = \mathcal{L}(\mathbf{x}) \end{aligned} \quad (6)$$

where $\mathbf{x} = (x_1, \dots, x_K)$ and $\mathbf{y} = (y_1, \dots, y_K)$. Then, our goal is to maximize the lower bound for the whole dataset \mathcal{D} :

$$\mathcal{L}(\mathcal{D}) = \frac{1}{N} \sum_{n=1}^N \mathcal{L}(\mathbf{x}^{(n)}) \quad (7)$$

This can be solved by the standard VAE techniques (stochastic variational Bayes, reparametrization, etc.; Kingma and Welling (2014)).

3.3 MLVAE

MLVAE differs from GVAE only in the way of inferring the content (equation 5), where the posterior distribution is estimated as the product of Gaussians for individual members (“evidence accumulation”):

$$q_\psi(z|x_1, \dots, x_K) = \frac{1}{Z} \prod_{k=1}^K \mathcal{N}(h_\psi(x_k), s_\pi(x_k)) \quad (8)$$

where Z is the normalizing constant. Since a product of Gaussians is a Gaussian, the above definition can be rewritten as:

$$(8) = \mathcal{N} \left(\frac{\sum_k h_{\psi}(x_k)/s_{\pi}(x_k)}{\sum_k 1/s_{\pi}(x_k)}, \frac{1}{\sum_k 1/s_{\pi}(x_k)} \right) \quad (9)$$

Note that the mean of the Gaussian has the form of weighted average where the weights are the precisions $1/s_{\pi}(x_k)$. Thus, MLVAE may appear to be more expressive than GVAE, which uses simple averaging (equation 5). However, GVAE is not a special case of MLVAE since the variance has a very different form.

Due to the weighted average form, the objective of MLVAE is significantly more complex than GVAE. Indeed, the form introduces multiplication and division between the outputs of deep nets, which makes optimization not easy. (This could be slightly simplified by letting a deep net represent the precision $1/s_{\pi}(x_k)$ instead of the variance $s_{\pi}(x_k)$, though). In fact, we often encountered training runs that resulted in two kinds of degenerate models, one with all $h(x)$ yielding 0 and the other with all $s(x)$ yielding 1. The first kind is clearly a failure in terms of disentangling, while the second kind makes no use of variance estimation and therefore defeats any potential advantage over GVAE. On the other hand, we did not have such difficulty in the case of GVAE.

4 Experimental set-up

We prepared the following three datasets. (1) Multi-PIE: multi-viewed natural face images derived from Gross et al. (2010). Grouping is done by the subject and (cloth/hair) fashion, while varying the view and expression. The training and test sets have disjoint 268 and 69 subjects. (2) Chairs: multi-viewed synthetic chair images derived from Schüldt et al. (2004). Grouping is done by the chairs type, while varying the view. The training and test sets have disjoint 650 and 159 types. (3) KTH: image frames from video clips of human (only pedestrian) motion derived from Schüldt et al. (2004). Grouping is done by the video clip id, while varying the position of the subject. The training and test sets have disjoint 20 and 5 subjects. See Appendix A for details of these datasets. Apart from these, we also tested smaller-sized datasets, but these generally produced rather poor disentangling results.

For each dataset, we built a GVAE model (Section 3.2) or an MLVAE model (Section 3.3) with convolutional neural nets for the encoders (g , r , h , and s) and a deconvolutional neural net as the decoder (f). We used the same architecture for all models with the transformation dimension $L = 3$ and the content dimension $M = 100$; See Appendix B for details of the

architecture. To train each model, we first randomly initialized the weight parameters of the encoders and decoder and then optimized the objective (7) (either using the inference distribution (5) or (9)) with respect to the weight parameters using the training set. Training proceeded by mini-batches (size 100), where each group was formed on the fly by randomly choosing 5 images according to the dataset-specific grouping strategy described above ($K = 5$). We used Adam optimizer (Kingma and Ba (2015)) with the recommended optimization parameters.

5 Results

5.1 Disentangling and generalizability

We started with a conventional qualitative evaluation of disentangling called swapping. In this, given two lists of inputs x_1, \dots, x_I and x'_1, \dots, x'_J , we show a matrix of images, each generated from the content representation estimated from an input x_i in the first list and the transformation representation estimated from an input x'_j in the second list: $f(g(x'_j), h(x_i))$. Note that we estimated the latent representation from a single image (with no grouping) and thus the encoders r and s were unused.

In Figure 2A, we show a swapping matrix for a GVAE model trained with Multi-PIE dataset. The top row and the left-most column show two lists of sample images in the training set. In the matrix, we can observe reasonably successful disentangling: each generated image reflects the subject of the corresponding input in the first list and the view of the corresponding input in the second list. Figure 2B shows a swapping matrix for sample test images. Generalization of disentangling to the test case can be observed with a quality more or less similar to the training case, which is remarkable, given the fact that none of the subjects here had been seen during the training.

Figure 2CD shows analogous swapping matrices for an MLVAE model also trained with Multi-PIE. Although the generated images were not the same as the GVAE model, the overall quality was quite similar. However, we will see a quantitative difference in Section 5.2. As another comparison, to examine whether grouping of data items was crucial, we redid the same experiment using a dataset with no group ($K = 1$). This case in fact corresponds to a basic VAE model with a single variable (Kingma and Welling (2014)) since, without grouping, the content and transformation variables can be integrated without loss of generality. The results clearly indicated failure of disentangling: no clear content-transformation separation could be observed and the generated images were often corrupted

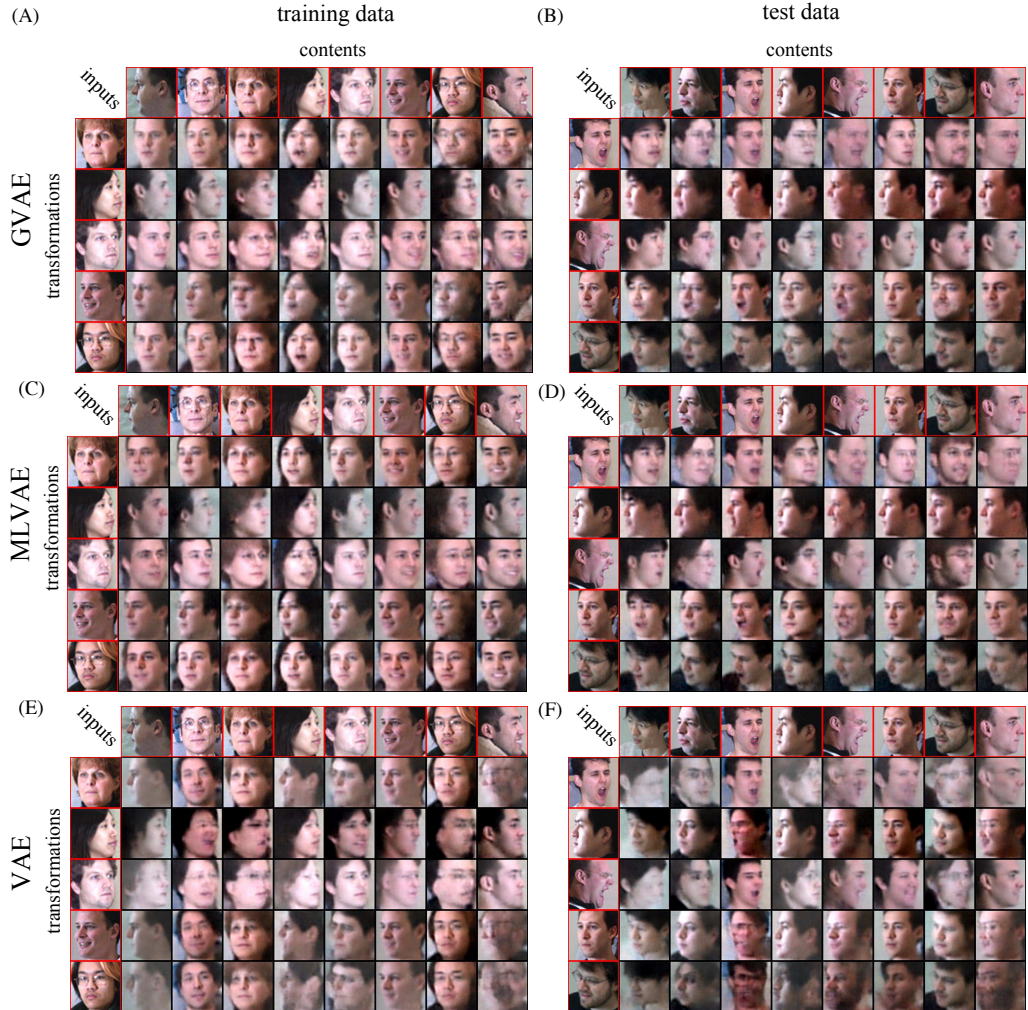


Figure 2: Qualitative evaluation of disentangling in models trained with Multi-PIE. (A,B) A swapping matrix from a GVAE model for training images (A) or test images (B). Each image in the matrix was generated from the content representation of a sample image in the top row and the transformation representation of another sample image in the left-most column. Red box: sample image. (C,D) Analogous swapping matrices from an MLVAE model. (E,F) Ditto from a VAE model.

(Figure 2EF).

We found that it was crucial for successful disentangling to choose a very low dimension for the transformation variable y (we used 3 dimensions here). This is because this variable would otherwise learn to represent all aspects of inputs including the contents and therefore the content variable z would become degenerate. Apart from this, we did not observe much effect from changes of other model parameters such as architectures of the encoders and decoders.

We conducted the same qualitative evaluation for models trained with Chairs or KTH datasets, each shown in Appendices C.2 and C.3. For both datasets, qualitative observations were similar: disentangling was generally

reasonable and generalizable to new contents; the qualities of the results were similar between the training and test cases and between GVAE and MLVAE models.

5.2 Few-shot classification

Since the qualitative evaluation did not reveal any difference between GVAE and MLVAE, we next conducted a quantitative evaluation by measuring performances of few-shot classification. The rationale is that, since the learned content representation is expected to eliminate information on transformation, this should allow for transformation-invariant recognition of objects. In particular, even for novel test classes, it should ideally be sufficient to hold the content representation of a

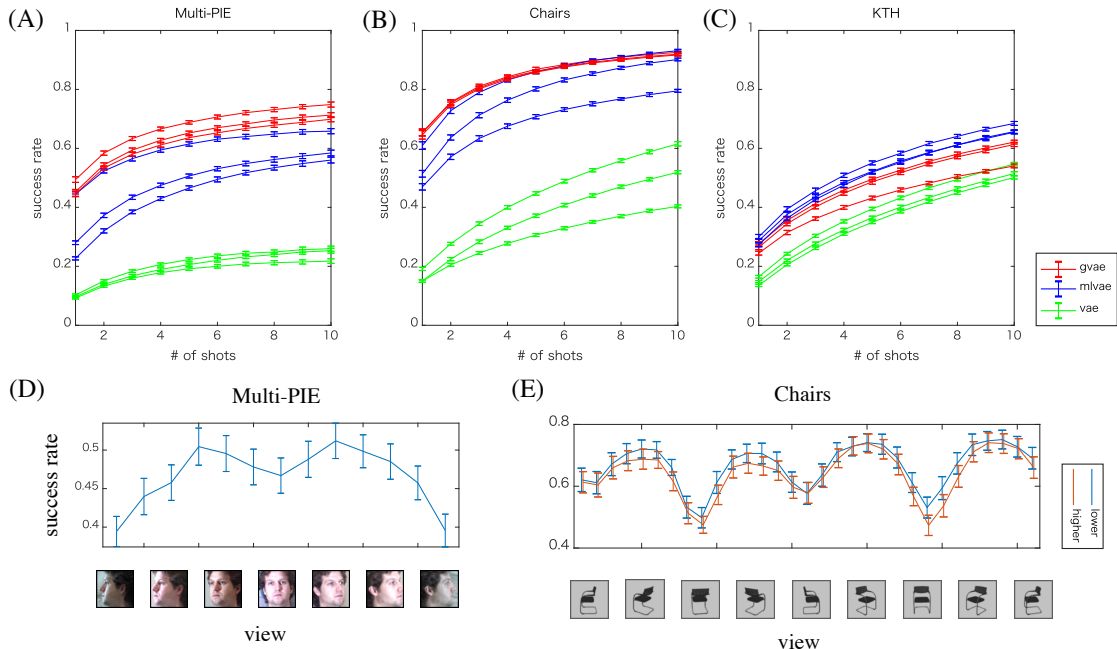


Figure 3: Quantitative evaluation of disentangling using few-shot classification. (A) The success rates (y-axis) of each model trained with Multi-PIE for different numbers of shots (x-axis). The error bars show the standard deviations across the splits. Three instances were examined for each method (legend). (B,C) Analogous results for Chairs and KTH. (D) The success rate (y-axis) for each view (x-axis) from a GVAE model trained with Multi-PIE. Two down-looking views are omitted. (E) Analogous result for Chairs. Two colors correspond to different vertical angles of view (legend).

single image for each class in order to classify the remaining images (one-shot learning). Thus, the better the disentangled representation is, the more accurate the few-shot classification should be.

Our evaluation procedure goes as follows. For a dataset, we formed 100 splits of gallery/probe of test images, where each gallery included S random images for each class and the corresponding probe included the remaining images. Here, a class refers to each subject/fashion combination in Multi-PIE (378 test classes), to each chair type in Chairs (159 test classes), and to each video clip in KTH (240 test classes). Then, for a trained model, we classified each probe image as the class of the gallery image that had the maximal cosine similarity with the input probe image in the space of content variable z ; classification succeeded if the inferred class matched the actual class. We measured success rates for each $S = 1, \dots, 10$ for each trained model. We compared three methods, GVAE, MLVAE, and VAE, where each model had the same encoder/decoder architectures (the VAE models were in fact GVAE models trained with ungrouped data). We examined three separately trained models for each method and each dataset.

Figure 3 summarizes the results. First, notice that performance variability across model instances was not negligible even within the same method, which means that comparing different methods by single instances would be meaningless. In particular, in the cases of Multi-PIE and Chairs, performance varied quite largely in MLVAE, possibly because the complex objective introduced many under-performing local optima.

The average performance of GVAE was higher compared to MLVAE in the cases of Multi-PIE and Chairs. However, in either case, the best performing MLVAE model was comparable with GVAE. This might mean that the best solution represented somewhat similar information on the content, but MLVAE had a more difficulty in finding such solution. We also found that the best performing MLVAE model for Multi-PIE (not the one shown in Section 5.1) was actually degenerate where the estimated variances $s(x)$ were always 1. This indicates that the evidence accumulation technique may not actually be so effective for generalizable disentangling; we return to this point in Section 5.3. However, these results are dependent on the dataset: MLVAE performed moderately better in the case of KTH.

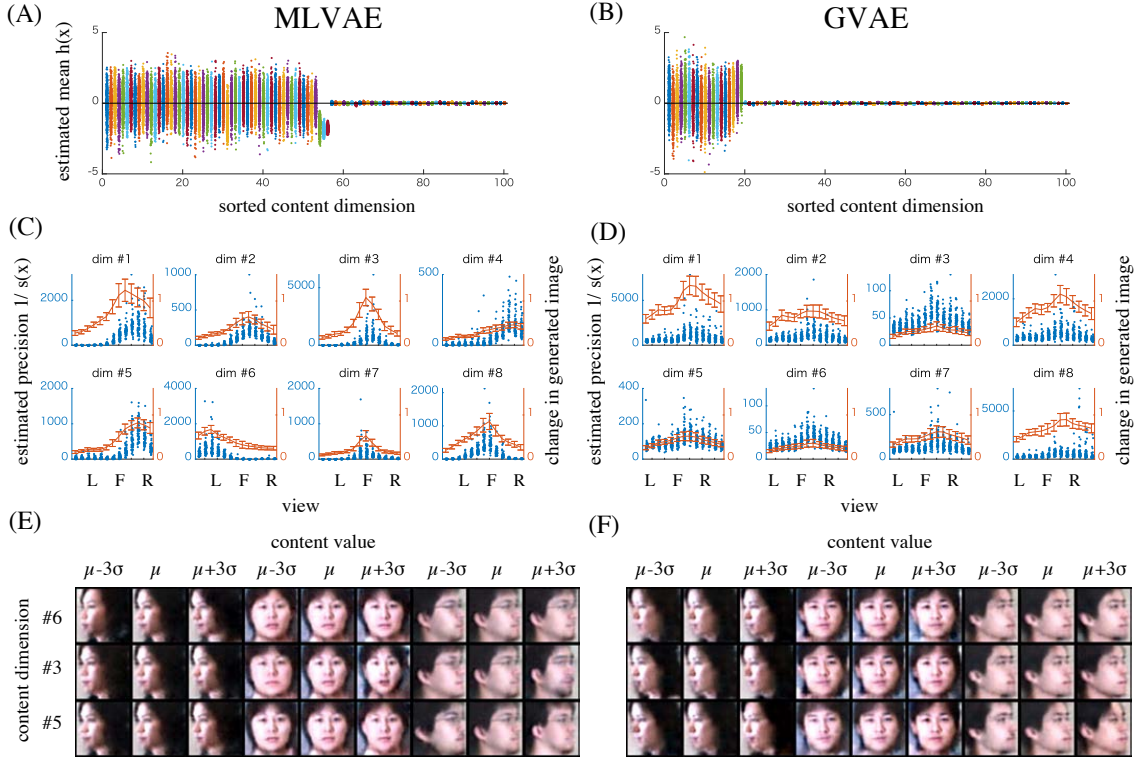


Figure 4: Analysis of latent content representations. (A) The distributions of estimated means $h(x)$ for each content dimension in an MLVAE model trained with Multi-PIE. The content dimensions are sorted according to the standard deviation. (C) Blue: the distributions of estimated precisions $1/s(x)$ for each view for each of top 8 content dimensions in the MLVAE model. Red: the view-wise normalized distances between two images generated from latent variables differing in one dimension. (E) The images generated from the latent representations of three sample images while varying the content dimension #6, #3, or #5 in the MLVAE model. The three sample images were chosen so that each gives a high estimated precision at one of the three content dimensions in the MLVAE model. (B,D,F) Analogous results for the GVAE model.

The VAE models generally performed quite badly compared to other methods. This is not surprising since the disentangled representations were qualitatively poor as shown in Figure 2EF.

As a side interest, we wondered which view of 3D objects led to more successful recognition. Figure 3DE show the view-wise success rates of one-shot classification in GVAE models. We found that, in both Multi-PIE and Chairs, diagonal views always gave better success rates than profile or frontal views. This result is intuitive since we can perceive better the entire shape of a face or chair from diagonal views than other views. Perhaps, this is the reason why photos of actors or furniture items are typically taken in diagonal views.

5.3 Encoding strategy of contents

To further understand the quantitative differences, we conducted some analyses on the latent content represen-

tation. First of all, Figure 4 plots the estimated mean values $h(x)$ of each content dimension for test images from an (A) MLVAE or (B) GVAE model trained with Multi-PIE, where the content dimensions are sorted by the standard deviation. In both, only a part of the full dimensions were effective and the rest became degenerate. However, the GVAE model used a much fewer dimensions. This tendency was generally observed in all other models we trained.

To see why, it is important to see view-specific structure in the estimated variances in each model. In Figure 4C, each scatter plot (blue) shows the estimated precisions $1/s(x)$ for each view (left-profile, frontal, right-profile, etc.) for one of top 8 content dimensions in the MLVAE model. The estimated precisions tended to be peaked at a particular view while they went down to very low values elsewhere, and the peak view was different from dimension to dimension. This was starkly different from the GVAE case (Figure 4D), where the estimated

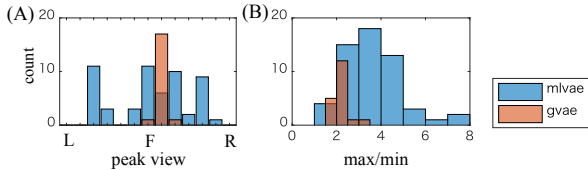


Figure 5: (A) The distribution of peak views (in terms of changes in generated images) for the effective dimensions in each model shown in Figure 4 (legend). (B) The distribution of ratios of maximum and minimum changes in generated images in each model.

precisions were only slightly higher for frontal views compared to profile views for most dimensions. Recall the weighted-average form in MLVAE (equation (9)), where each estimated mean is multiplied with the corresponding estimated precision. Since the estimated precisions were very low in the non-peak views, we would expect that the content dimension tended to have particularly strong meaning around the peak views.

To confirm this, we estimated the latent variables for each test image and generated two new images using the same variables but modifying one dimension of the content variable to either a small value ($\mu - 3\sigma$ using the mean μ and s.d. σ of $h(x)$ for that dimension) or a large value ($\mu + 3\sigma$); we then calculated the normalized Euclidean distance between the two new images. In Figure 4CD, each curve (red) shows such distances for each view for one content dimension. We can see that the distances consistently followed the magnitudes of precisions in both cases. As a consequence, in MLVAE, each dimension had much more influence on the generated images in high-precision views than low-precision views, whereas the contrast was more moderate in GVAE (Figure 5B). Also, note that the peak views covered a broad range in MLVAE, while they were concentrated around the frontal view (Figure 5A).

To illustrate, we chose three sample images of left-profile, frontal, and right-profile views that elicited large precisions values for dimensions #6, #3, and #5, respectively, in the MLVAE model (each emphasizing left-profile, frontal, and right-profile views). Figure 4E shows generated images from the three images in the MLVAE model, while varying those three dimensions. We can observe that changes of images tended to be larger for views with high precisions. For example, varying dimension #6 led to large changes in the left-profile view, but small changes in the other views. Figure 4F shows analogously generated images for the GVAE model, but changes in all content dimensions tended to alter the generated images equally in all views.

This view-dependent coding in MLVAE may explain the larger number of effective dimensions in MLVAE (Figure 4AB). It is perhaps because different dimensions were used for representing different views and therefore encoding of all views would require a larger number of dimensions than GVAE, in which each dimension seemed to play a role in all views.

The view dependency of the estimated precisions may be related to uncertainty coding of facial features. That is, since a single image provides only partial information for the content, the inference necessarily includes ambiguity. For example, from a frontal face image, we are sure about the eyes, nose, and mouth, but less sure about the ears; from a profile face image, we are sure about the visible side of the face, but much less sure about the invisible side. Thus, we might be able to infer a more accurate content representation if we integrate estimated content information for different views with the uncertainty taken into account. However, the view-dependent representation seems to go somewhat in the opposite direction to the goal of disentangling—to discover view-invariant representation—which might be one explanation for the observed lower performance of MLVAE in few-shot classification.

6 Conclusion

To investigate a probabilistic method for learning generalizable disentangled representations, we proposed group-contrastive VAE, which exploits grouping structure in a dataset to extract the content as the common factor and the transformation as the remaining factor. Our approach achieved, for three datasets, effective disentangling of content and transformation and generalizes for test images with new contents. While qualitative comparison indicated little difference from MLVAE, quantitative comparison using few-shot classification showed superiority for some datasets. Our detailed analysis of the content representation revealed transformation-dependent coding arising from the evidence accumulation technique in MLVAE, which may potentially conflict with the goal of disentangling.

Acknowledgments

The author expresses special thanks to Aapo Hyvärinen, Mohammad Emtiyaz Khan, and Motoaki Kawanabe for precious comments and suggestions. This work has been supported by Grants-in-Aid for Scientific Research.

References

Bouchacourt, D., Tomioka, R., and Nowozin, S. (2018). Multi-Level Variational Autoencoder: Learning Dis-

-
- entangled Representations from Grouped Observations. In *AAAI Conference on Artificial Intelligence*.
- Chen, M., Denoyer, L., and Artières, T. (2018). Multi-View Data Generation Without View Supervision. In *International Conference on Learning Representations*.
- Chen, X., Duan, Y., Houthoofd, R., Schulman, J., Sutskever, I., and Abbeel, P. (2016). InfoGAN - Interpretable Representation Learning by Information Maximizing Generative Adversarial Nets. *Advances in neural information processing systems*.
- Cheung, B., Livezey, J. A., Bansal, A. K., and Olshausen, B. A. (2014). Discovering Hidden Factors of Variation in Deep Networks. In *International Conference on Learning Representations, Workshop*.
- Denton, E. and Birodkar, V. (2017). Unsupervised Learning of Disentangled Representations from Video. *Advances in neural information processing systems*.
- Dosovitskiy, A. and Springenberg, J. T. (2015). Learning to generate chairs with convolutional neural networks. In *The IEEE Conference on Computer Vision and Pattern Recognition*.
- El Shafey, L., McCool, C., Wallace, R., and Marcel, S. (2013). A scalable formulation of probabilistic linear discriminant analysis: applied to face recognition. *IEEE Transactions on Pattern Analysis and Machine Intelligence*, 35(7):1788–1794.
- Földiák, P. (1991). Learning invariance from transformation sequences. *Neural Computation*, 3(2):194–200.
- Goodfellow, I., Pouget-Abadie, J., and Mirza, M. (2014). Generative adversarial nets. *Advances in neural information processing systems*.
- Gross, R., Matthews, I., Cohn, J., Kanade, T., and Baker, S. (2010). Multi-PIE. *Proceedings of the International Conference on Automatic Face and Gesture Recognition. IEEE International Conference on Automatic Face & Gesture Recognition*, 28(5):807–813.
- Higgins, I., Matthey, L., Pal, A., Burgess, C., Glorot, X., Botvinick, M., Mohamed, S., and Lerchner, A. (2016). beta-VAE: Learning Basic Visual Concepts with a Constrained Variational Framework. In *International Conference on Learning Representations*.
- Kingma, D. and Ba, J. (2015). Adam: A method for stochastic optimization. In *International Conference on Learning Representations*.
- Kingma, D. P., Mohamed, S., and Rezende, D. J. (2014). Semi-supervised learning with deep generative models. *Advances in neural information processing systems*.
- Kingma, D. P. and Welling, M. (2014). Auto-encoding variational bayes. In *International Conference on Learning Representations*.
- Mathieu, M., Zhao, J. J., Sprechmann, P., Ramesh, A., and LeCun, Y. (2016). Disentangling factors of variation in deep representation using adversarial training. *Advances in neural information processing systems*.
- Schüldt, C., Laptev, I., and Caputo, B. (2004). Recognizing Human Actions - A Local SVM Approach. In *International Conference on Pattern Recognition*, pages 32–36 Vol.3. IEEE.
- Siddharth, N., Paige, B., van de Meent, J.-W., Desmaison, A., Wood, F., Goodman, N. D., Kohli, P., and Torr, P. H. S. (2017). Learning Disentangled Representations with Semi-Supervised Deep Generative Models. *Advances in neural information processing systems*.
- Yang, J., Reed, S., Yang, M.-H., and Lee, H. (2015). Weakly-supervised Disentangling with Recurrent Transformations for 3D View Synthesis. *Advances in neural information processing systems*.

Appendix

A Dataset details

Multi-PIE The original dataset (Gross et al. (2010)) consists of natural face images of 337 subjects in 15 views, with 3 expressions, and in 4 (cloth/hair) fashions. We used only images under illumination of a medium brightness (condition 9) and cropped and resized them using the manually annotated landmark positions provided by El Shafey et al. (2013) ($64 \times 64 \times 3$ pixels). We split the data into a training set with $\sim 32\text{K}$ images of 268 subjects and a test set with $\sim 6\text{K}$ images of the remaining 69 subjects. We formed each group by randomly choosing face images of the same subject and fashion, but varying the view and the expression.

Chairs The original dataset (Dosovitskiy and Springenberg (2015)) consists of synthetic multi-viewed chair images of various types rendered from 3D models. We used a convenient dataset prepared by Yang et al. (2015), which includes images ($64 \times 64 \times 3$ pixels) of 809 chair types in 62 different views (31 horizontal and 2 vertical angles). We split the data into a training set with $\sim 40\text{K}$ images of 650 chair types and a test set with $\sim 10\text{K}$ images of the remaining 159 chair types. We formed each group by randomly selecting chair images of the same type but varying the view.

KTH The original dataset (Schüldt et al. (2004)) consists of video clips of human motion of 6 types by 25 subjects, where each clip shows one type of motion by a single subject with varied settings (background, motion direction, cloth, camerawork, etc.). From a subset with pedestrian motions (walking, running, and jogging), we created a training set with image frames (64×64 pixels) from 960 video clips of 20 subjects and a test set with image frames from 240 video clips of the remaining 5 subjects; we removed frames showing no person. We formed each group by randomly selecting image frames in the same video clip.

B Architecture details

Each model used convolutional neural nets as the encoders (g , r , h , and s) and a deconvolutional neural net as the decoder (f). Each encoder had three convolution layers with 64 filters (kernel 5×5 ; stride 2; padding 2) followed by two fully connected layers (64 units/3 units for g and r ; 100 units/100 units for h and s). The decoder f had two fully connected layers (103 units/128 units) followed by three transposed convolutional layers with 64 filters (kernel 6×6 ; upsampling 2; cropping 2). An RELU layer was inserted between convolutional or fully connected layers; the encoders r and s had an additional nonlinearity layer after the top layer to ensure positivity: $F(a) = \exp(a/2)$. Only for an MLVAE model, we let the deep net s encode the precision instead of the variance.

C Additional results

C.1 Multi-PIE

In addition to swapping, we conducted qualitative evaluation using interpolation: given two inputs x_1 and x_2 , we show a matrix of images, each generated from a linear interpolation of the content and transformation representations estimated for both inputs: $f((1 - \beta)g(x_1) + \beta g(x_2), (1 - \alpha)h(x_1) + \alpha h(x_2))$ for $0 \leq \alpha, \beta \leq 1$; extrapolation is also possible with α, β outside this range.

Figure 6AB shows an interpolation matrix in a GVAE model for a pair of sample training (A) or test images (B), in which the generated images in each row linearly varied the content variable while fixing the transformation variable; those in each column were converse. Note the smooth transition of the generated images in both axes. We also show the generated images for extrapolated contents; note that some facial features (e.g., hair) were exaggerated. Although interpolation in transformation was reasonable in the shown examples, we found that it was not generally the case when the input images had very different views. Figure 6CD

shows analogous matrices for an MLVAE model; the results were qualitatively similar to the GVAE model.

C.2 Chairs

Figure 7 shows swapping matrices and interpolation matrices for sample training or test images, in a GVAE or MLVAE model trained for Chairs dataset; the formats are the same as Figure 2 and Figure 6. For this dataset, the expected content and transformation were the chair type and the view, respectively. Disentangling was quite successful and generalizable to new chair types; the quality was more or less the same in both training and test cases and in both GVAE and MLVAE models.

C.3 KTH

Figure 8 shows analogous results for KTH dataset. For this data, the expected content was the subject, motion type, and other settings, while the expected transformation was the position of the subject. Again, reasonable disentangling can be observed in both the training and test cases, though the subject was not very clear due to the quality of generated images. Also, moderate degrading in the test case can be observed. Interpolation and extrapolation in the transformation axis were generally clean.



Figure 6: Interpolation matrices from GVAE and MLVAE models trained with Multi-PIE. An interpolation matrix for a pair of sample training images (A,C) or test images (B,D), where the content variables were interpolated and extrapolated in rows and the transformation variables were interpolated in columns. Green box: image corresponding to an input.

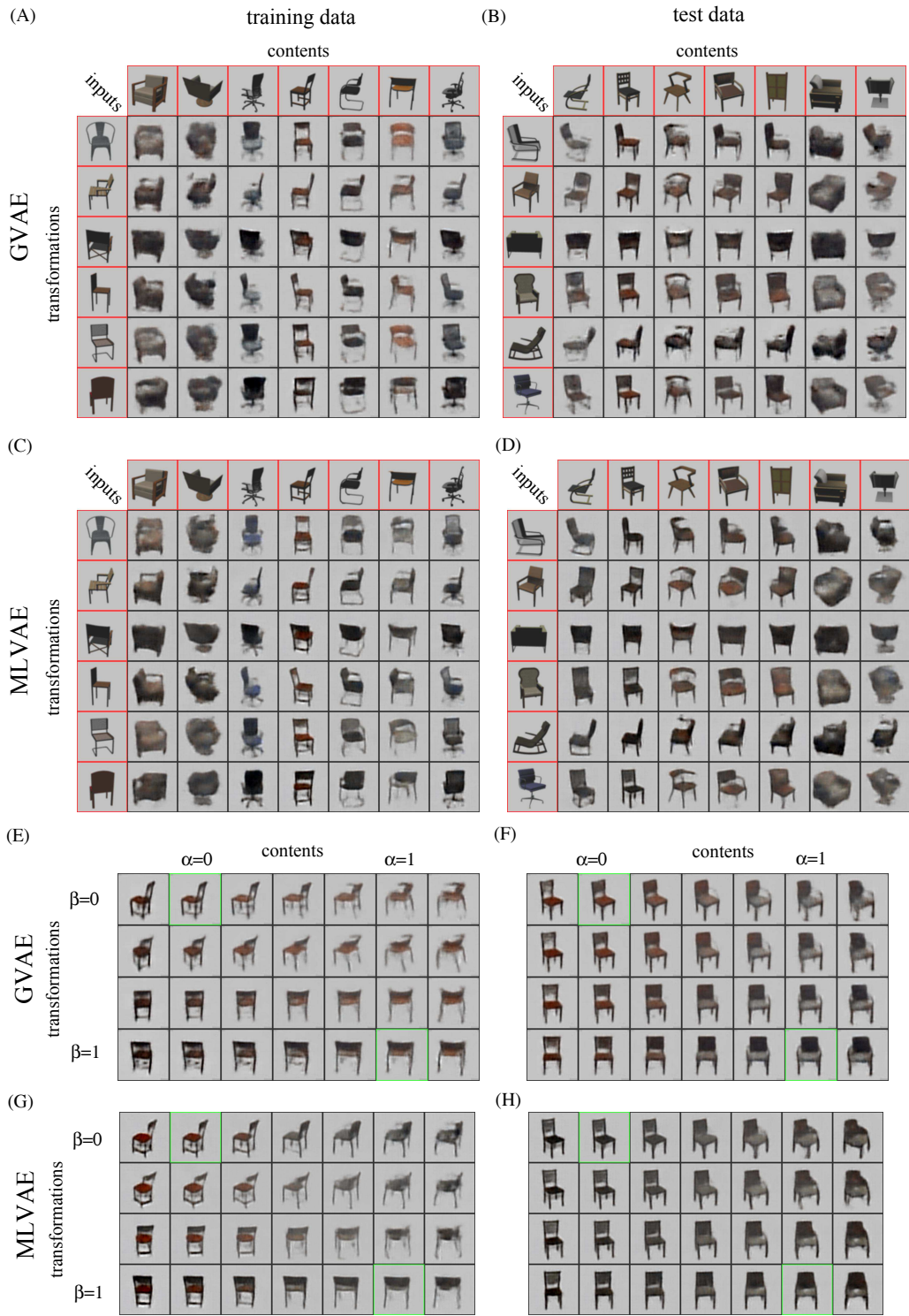


Figure 7: Swapping and interpolation matrices from GVAE and MLVAE models trained with Chairs.

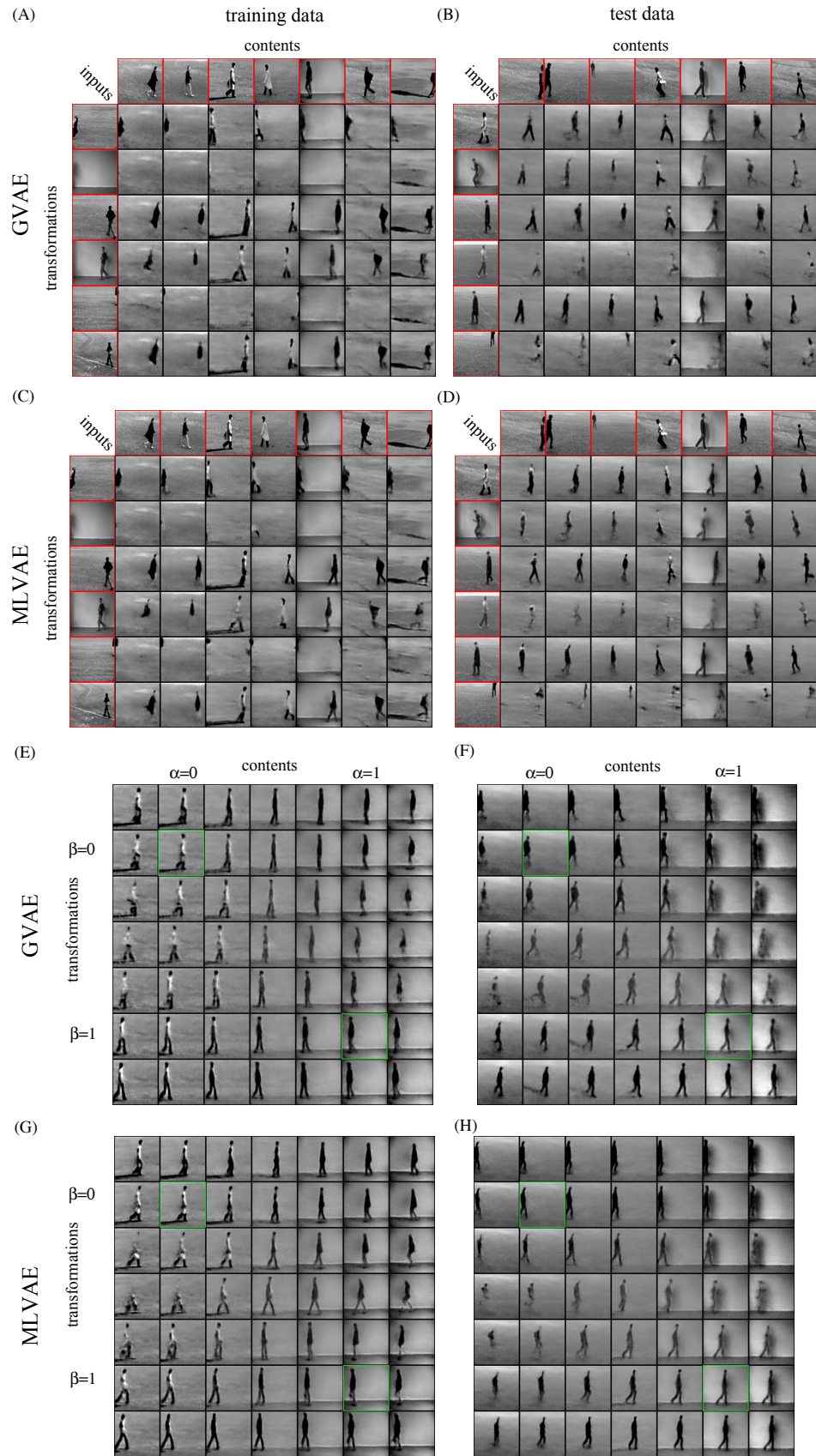


Figure 8: Swapping and interpolation matrices from GVAE and MLVAE models trained with KTH.